Hydrogen-Bond Dynamics in a Protic Ionic Liquid: Evidence for Large-Angle Jumps

Johannes Hunger,[a,b,*] Thomas Sonnleitner,[c] Liyuan Liu,[a] Richard Buchner,[c] Mischa Bonn,[a,b] and Huib J. Bakker[a]

[a] FOM Institute AMOLF, Science Park 104, 1098 XG Amsterdam, The Netherlands

[b] Max Planck Institute for Polymer Research, Ackermannweg 10, 55128 Mainz, Germany, hunger@mpip-mainz.mpg.de

[c] Institut für Physikalische und Theoretische Chemie, Universität Regensburg, Universitätsstraße 31, 93053 Regensburg, Germany

[*] to whom correspondence should be addressed

Abstract

We study the molecular rotation of the protic room temperature ionic liquid ethylammonium nitrate (EAN) with dielectric relaxation spectroscopy and femtosecond-infrared spectroscopy (fs-IR) of the ammonium N-H vibrations. The results suggest that the rotation of ethylammonium ion takes place via large angular jumps. Such non-diffusive reorientational dynamics is unique to strongly hydrogen-bonded liquids such as water, and indicates that the intermolecular interaction is highly directional in this class of ionic liquids.

TOC Figure

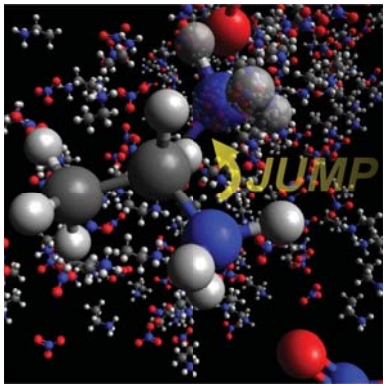

Keywords

time-resolved infrared spectroscopy – dielectric spectroscopy – liquid dynamics – molecular rotation – ethylammonium nitrate

Ethylammonium nitrate ($C_2H_5NH_3^+$ NO_3^-; EAN) is the first reported room temperature ionic liquid (RTIL), having been discovered already in 1914.[1] EAN is formed via neutralization of a Brønsted acid with a corresponding base and thus belongs to a subset of RTILs: protic ionic liquids (PILs).[2] PILs have unique solvent properties akin to typical aprotic RTILs, however, they can form very strong hydrogen-bonds. The hydrogen-bonded nature of PILs is thought to promote the aggregation of amphiphilic molecules,[2] and may explain the extraordinarily high charge mobilities due to a Grotthuss type hopping mechanism.[3] Further, the strong hydrogen-bond interactions may result in the ability of PILs to dissolve proteins and enzymes while preserving their biological activity.[4]

Although the strong interaction between the constituting ions of PILs is evident from their far-infrared spectra,[5,6] NMR chemical shifts,[7,8] and from scattering experiments,[9] the presence of directional inter-ionic interactions, which would be characteristic for hydrogen bonding, has only been inferred indirectly from experiments. In fact, the interaction potentials for conventional RTILs are rather shallow,[10] and firm experimental evidence for directional inter-ionic interaction is lacking. Generally, for hydrogen-bonded liquids, water being the most prominent example, the hydrogen-bonded nature is unequivocally reflected in the rotational dynamics of the molecules. Specifically, the presence of directional H-bonds has as a consequence that the molecular reorientation is not simply diffusive, but instead occurs in a jump-like fashion.[11,12]

We study the molecular rotation in EAN using two complementary approaches. In the first approach we measure the frequency dependent response of EAN to an external electric field (dielectric spectroscopy, DS[13]) yielding the reorientation dynamics of molecular-level electric dipoles. Complementary to these experiments, we use femtosecond-infrared spectroscopy (fs-IR)[14,15] to measure the reorientation of the ammonium groups of EAN.

In DS[13] we measure the electrical polarization of EAN as a function of the field frequency, ν. The polarization of the sample is generally expressed in terms of the complex

permittivity, $\hat{\varepsilon} = \varepsilon' - \mathrm{i}\varepsilon''$, where ε' and ε'' correspond to the in-phase (dispersive) and out-of-phase (absorptive) polarization components, respectively. At GHz frequencies the polarization is predominately due to the rotation of the dipolar ions of the PIL.[16] For EAN the rotation of the nitrate anion does not contribute due to its symmetry-imposed zero net-dipole moment. The rotational relaxation of the cations leads to a characteristic peak in ε'' (Fig. 1a).[17–19] The peak frequency, $\nu_{\max}$ is characteristic for the rotation of the dipolar $C_2H_5NH_3^+$ cations. We extract the corresponding τ_{DR} ($= 1/2\pi\nu_{\max}$) from the experimental spectra by fitting an asymmetrically broadened relaxation model to the permittivity spectra (for details see Supporting Information, SI). As can be seen in Fig. 1a the relaxation band is centred at 700 MHz ($\tau_{\mathrm{DR}} = 212$ ps) at 5 °C. As the temperature increases, the band gradually shifts to higher frequencies, peaking at 4 GHz ($\tau_{\mathrm{DR}} = 41.5$ ps) at 65 °C, meaning that the rotational dynamics get accelerated with increasing temperature. The speed-up of τ_{DR} with increasing temperature is excellently described by an Arrhenius type equation (Fig. 1b).

We compare the DS results to the results of fs-IR experiments. In the latter experiments a molecular group is tagged via excitation of an intrinsic vibration with an intense infrared laser pulse, after which the reorientation of this group can be followed in time with subsequent infrared pulses. In the present study we exchange some of the NH groups of the ethylammonium ion by ND ($[C_2H_5NH_{3-x}D_x]^+$; $x = 0 \ldots 0.286$) groups resulting in $[C_2H_5NH_2D]^+$ ions as the prevailing deuterated species in the samples (see SI). We use the ND group, with its stretching vibration centred at 2290 cm^{-1} (Figs. 2 & S1) as the molecular probe. Excitation of the ND vibration leads to a transient change in the infrared absorption spectrum, $\Delta\alpha_{\mathrm{iso}}$. We probe these transient absorption changes as a function of time, t, using a second delayed weak infrared probe pulse. In Fig. 2 we show the thus induced isotropic absorption change. This absorption change is dominated by a bleaching signal ($\Delta\alpha_{\mathrm{iso}} < 0$) at 2250 cm^{-1} due to the population of the first excited vibrational state

and the accompanied depletion of the vibrational ground state population and stimulated emission of the excited state shortly after the excitation. The dynamics of this isotropic absorption change is independent of reorientation processes and represents only the vibrational relaxation. The bandwidth of the bleach is significantly narrower than the ND absorption band and corresponds to the pump pulse bandwidth. This bleach does not broaden significantly (spectral diffusion) at short delay times ($t \leq 1\,\mathrm{ps}$; Fig. 2a). This indicates that on short timescale ($\sim 1\,\mathrm{ps}$) the local structure of EAN is heterogeneous and quasi-static. Fluctuations of the ND absorption frequency apparently take place on appreciably longer timescales. At $\sim 2100\,\mathrm{cm}^{-1}$ we observe an adjacent induced absorption ($\Delta\alpha_{\mathrm{iso}} > 0$) due to the excited state absorption ($1 \rightarrow 2$ transition).

In Fig. 2b we show the evolution of the bleaching signal at $2250\,\mathrm{cm}^{-1}$ as a function of the delay time. A detailed analysis (see SI) yields a vibrational lifetime of $\tau_1 = (200 \pm 40)\,\mathrm{fs}$ of the excited state population that is independent of temperature and x. At intermediate times, $1\,\mathrm{ps} < t < 10\,\mathrm{ps}$ a second, slower component in the $\Delta\alpha_{\mathrm{iso}}$ signal recovery is observed, which is most prominent for $x \leq 0.068$ (Figs. 2b & S2). The absence of any signature of this relaxation component in the excited state absorption at $\omega = 2085\,\mathrm{cm}^{-1}$ (Fig. S2) suggests that the ND excitation decays via an intermediate energy level that is transiently populated, e.g. a vibration of the NH_2D^+ group.[20] A similar relaxation mechanism has been observed for liquid ammonia,[21] for which the relaxation of the N-D vibration was observed to proceed via the scissoring vibration of the NH_2D group. The intermediate state relaxes with a time constant of $\tau_2 = (2.5 \pm 0.6)\,\mathrm{ps}$ to lower energy levels. This second relaxation is independent of temperature and isotope exchange ratio x. The occupation of these lower levels results in a persistent non-zero end level of the change in absorption. This persistent absorption change corresponds to a blue-shift of the ND band (i.e. $\Delta\alpha_{\mathrm{iso}}$ that results from a rise in temperature of the sample by a few degrees, see SI Fig. S4). However, as can be seen in Fig. 2b the structure of EAN cannot adopt instantaneously to the local thermal

disturbance, as the final equilibrium is only reached at $t > 50\,\mathrm{ps}$. These slow thermalization dynamics go along with an increase of the magnitude of $\Delta\alpha_{\mathrm{iso}}$, while the spectral shape (i.e. the thermal difference spectrum) is unaffected. Thus, these slow dynamics are likely related to the structural rearrangement of the three-dimensional structure of EAN and presumably contain substantial translational motion. The timescale of the thermalization dynamics exhibits a distinct temperature dependence ($\tau_3 = (15.7 \pm 1.2)$, (13.4 ± 2.4), and (11.7 ± 0.9) ps at 25, 45, and 65 °C, respectively), which indicates that the three-dimensional RTIL structure becomes more flexible when the temperature increases.

As will be shown below, the effect of the vibrational excitation remains localized on relatively long timescales ($> 10\,\mathrm{ps}$), although the vibrational excitation itself decays quickly. This fact allows us to follow the liquid dynamics over long timescales. Specifically, we can follow molecular reorientation in real time. Vibrational excitation occurs most efficiently for ND groups that have their transition dipole aligned with the laser polarization. Hence, the vibrational excitation will be anisotropic. This anisotropy will decay as a result of molecular rotations. The anisotropy parameter, R, is defined by the normalized difference between the absorption change parallel and perpendicular to the pump polarization. As can be seen from Fig. 3, we observe a surprisingly long-lived (10's of ps) anisotropy in the induced absorption changes that shows a remarkable dependence on the isotopic exchange ratio, x. This long-lived anisotropy cannot be associated with vibrationally excited N-D groups because the vibrational excitation rapidly decays. Apparently, even after vibrational relaxation, some memory of the orientation of the initially excited ND vibration is retained. This observation can be explained from the fact that the vibrational relaxation will lead to a local dissipation of energy near the originally excited ND oscillators. Hence, the rise in temperature resulting from the vibrational relaxation is initially only affecting the originally excited ND oscillators, which implies that the thermal difference spectrum retains the anisotropy of the original vibrational excitation. Thus, our results show that the

dissipated thermal energy is initially distributed within the direct solvation shell. Owing to the slow thermal diffusion in EAN, we observe the anisotropy of these 'thermally' labelled ND groups. This provides a rather unique opportunity to measure the rotational dynamics over time scales that are much longer than the lifetime of the vibrational excitation.

As t increases, the anisotropy of the thermal label can decay via two different mechanisms. Firstly, the thermal energy diffuses from the excited ND group to other non-excited, randomly oriented ND oscillators. This effect is strongly dependent on the average distance between the ND groups and explains the increase of the decay rate of $R(t)$ with decreasing average distance (increasing exchange ratios) between the ND groups (Fig. 3). At high values of x, the decay of $R(t)$ is dominated by this thermal diffusion effect and the observed $R(t)$ decays do not vary significantly with temperature (Fig. 3, $x = 0.286$). Secondly, $R(t)$ will decay as a result of the rotation of the excited ammonium groups. This contribution dominates for low values of x for all delay times, and for large values of x for long delay times, as the progressive thermal diffusion leads to a decrease of the local thermal gradients. To quantify both contributions, we model[22] the experimental $R(t)$ decays (for details see SI) using a continuum heat diffusion model. In this model the dissipation of the vibrational energy leads to a heating of the direct environment of a ND oscillator (radius P). From this heated spot, the energy diffuses to the surrounding bath. The diffusing energy will only lead to a change of the anisotropy once it reaches other ND oscillators that absorb in the same frequency range. The number density of these, not excited and isotropically oriented ND oscillators is defined by the isotopic exchange ratio x. The ratio between the thermal energy experienced by the originally excited ND vibration and the excess thermal energy of all ND bonds can be readily related to $R(t)$. In addition, $R(t)$ decays due to the rotation of the excited ND oscillator. We fit this model to all $R(t)$ decays at each temperature simultaneously, where the heat diffusivity, χ, the rotation time, τ_{IR}, and the radius, P, are the global fit parameters. We find that this model with only

three independent parameters provides an excellent description of all measured $R(t)$ decays (Figs. 3 & S5). The slight deviations observed at early delay times likely originate from the fact that the continuum model does not include any molecular level structure.

From the fit of this model to the experimental anisotropies at 25 °C we obtain a thermal diffusivity of $\chi = (2.1 \pm 0.1)\,\text{Å}^2\text{ps}^{-1}$, which is five times lower than the macroscopic value ($\chi = 11\,\text{Å}^2\text{ps}^{-1}$).[23] This discrepancy may be due to the different character of the energy levels that are involved in the vibrational relaxation compared to macroscopic heat transport in a continuum.[22] The discrepancy may also be due to the local molecular heterogeneity in EAN.[24]

For the radius of the thermally excited spot we extract a value of $P = (6.5 \pm 1.7)\,\text{Å}$. This value of P is consistent with the energy being dissipated within the excited ND group and its closest shell of neighboring ions. The obtained rotational correlation time corresponds to $\tau_{\text{IR}} = (80 \pm 8)\,\text{ps}$ at 25 °C. Increasing the temperature to 45 °C leads to minor changes of the thermal diffusivity and the radius ($\chi = (2.3 \pm 0.4)\,\text{Å}^2\text{ps}^{-1}$; $P = (5.4 \pm 1.2)\,\text{Å}$). In contrast, the molecular rotation time is strongly accelerated ($\tau_{\text{IR}} = (48 \pm 12)\,\text{ps}$). This is also directly evident from the raw data from the much steeper decay of $R(t)$ at long delays ($t > 30$ ps) compared to the results at 25 °C (Fig. 3). The same notion applies to the anisotropies measured at 65 °C ($\chi = (2.2 \pm 0.4)\,\text{Å}^2\text{ps}^{-1}$; $P = (5.8 \pm 1.3)\,\text{Å}$, $\tau_{\text{IR}} = (28 \pm 6)\,\text{ps}$) (see SI). Therefore, while the heat diffusivity is essentially temperature independent, we observe a strong increase of the rotational mobility with increasing temperature. The obtained τ_{IR} values follow an Arrhenius type equation (Fig. 1b) with an activation energy of $E_{\text{A}}(\tau_{\text{IR}}) = (21.4 \pm 0.6)\,\text{kJ mol}^{-1}$, which coincides with $E_{\text{A}}(\tau_{\text{DR}})$. Both values of E_{A} are similar to the thermal activation of transport properties, like the viscosity.[17]

The good agreement of $E_{\text{A}}(\tau_{\text{IR}})$ with $E_{\text{A}}(\tau_{\text{DR}})$ is not self-evident, as the two experiments probe the rotation of a different vector of the ethylammonium ion. Fs-IR spectroscopy measures the rotation of the NH (ND) bond, while DS probes the effects of dipolar reorienta-

tions on the macroscopic polarization. In principle the ND group could show an additional local reorientation dynamics within the (immobile) ethylammonium cation. However, our present results suggest that such a fast rotation around the C-N axis does not significantly contribute to our fs-IR results, indicating the strong interaction of the N-D groups with its environment. In fact, the excellent agreement of the activation energies indicates that the two experiments are probing the same dynamical process, i.e. the rotation of the ethylammonium cations. The ratio $\tau_{\mathrm{DR}}/\tau_{\mathrm{IR}} \approx 1.4$ is actually surprisingly small in view of the fact that fs-IR probes the second-order rotational correlation time while the DS experiments probe the first order rotational correlation time. In the case of nonspecific interactions between the rotating molecule with the surrounding medium, i.e. diffusive reorientation via infinitely small angle rotations, a ratio of $\tau_{\mathrm{DR}}/\tau_{\mathrm{IR}} = 3$ is expected.[26]

In fact, for liquid ammonia the ratio of the second-order rotation time for the rotation of the N-H bond and the dielectric relaxation time is almost exactly 3 (cf. Refs. 27 and 28). The striking difference with respect to EAN is the absence of a strong hydrogen-bond acceptor molecule (i.e. the NO_3^- anion). Here, we observe a very small ratio $\tau_{\mathrm{DR}}/\tau_{\mathrm{IR}} \approx 1.4$ for the ethylammonium ion. The plausible explanation for this small ratio is the strong interaction between the ions, which cause the reorientational motion to be highly cooperative, involving the collective rearrangement of neighboring ions.[16,29] In analogy to water reorientation,[12] the rotation of $C_2H_5NH_3^+$ ion may thus take place via large angular jumps, as has been suggested previously for aprotic RTILs.[30,31] In water, the molecular reorientation was found to involve the concerted cleavage and re-formation of hydrogen-bonds to neighbouring water molecules.[11,12] The water reorientational jump angle was found to be $\sim 60\,^\circ$, which leads to a ratio of the first and the second-order rotational correlation time of ~ 2.[30,31] The observed ratio $\tau_{\mathrm{DR}}/\tau_{\mathrm{IR}}$ of 1.4 for EAN corresponds to a jump angle $\alpha \approx 106\,^\circ$,[25,32] assuming jumps about a unique angle. This angle closely resembles the tetrahedral angle of the ammonium group. Thus, the presence of highly

directional hydrogen-bonds formed between the $C_2H_5NH_3^+$ ion and NO_3^- ion in the ionic liquid is the likely reason for the small τ_{DR}/τ_{IR} ratio of 1.4, which is consistent with the hydrogen-bonds making the potential energy surface around the cation very anisotropic and the distribution of hydrogen-bond angles rather narrow.[33] Further experimental and theoretical studies, in particular molecular dynamics simulations, will be needed to confirm this picture. In particular, MD simulations may give more insight in the interplay between the ethylammonium cation and the nitrate ion in determining the orientational motions of both ions.

Acknowledgment

This work is part of the research program of the *Foundation for Fundamental Research on Matter (FOM)*, which is part of the *Netherlands Organisation for Scientific Research (NWO)* and it was funded by the *Deutsche Forschungsgemeinschaft* (DFG) within Priority Program 1191. JH thanks the DFG for funding through the award of a research fellowship.

Supporting Information Available

Additional material describing the experimental details, data analysis, and showing some supporting figures is available free of charge via the Internet http://pubs.acs.org.

References

(1) Walden, P. Molecular Weights and Electrical Conductivity of Several Fused Salts. *Bull. Acad. Impér. Sci. St. Pétersbourg* **1914,** *8,* 405-422.

(2) Greaves, T. L.; Drummond, C. J. Protic Ionic Liquids: Properties and applications. *Chem. Rev.* **2008,** *108,* 206-237.

(3) Angell, C. A.; Byrne, N.; Belieres, J. P. Parallel developments in Aprotic and Protic Ionic Liquids: Physical Chemistry and Applications. *Acc. Chem. Res.* **2007,** *40,* 1228-1236.

(4) Kragl, U.; Eckstein, M.; Kaftzik, N. Enzyme Catalysis in Ionic Liquids. *Curr. Opin. Biotechnol.* **2002,** *13,* 565-571.

(5) Fumino, K.; Wulf, A.; Ludwig, R. Hydrogen Bonding in Protic Ionic Liquids: Reminiscent of Water. *Angew. Chem. Int. Ed.* **2009,** *48,* 3184-3186.

(6) Fumino, K.; Reichert, E.; Wittler, K.; Hempelmann, R.; Ludwig, R. Low-Frequency Vibrational Modes of Protic Molten Salts and Ionic Liquids: Detecting and Quantifying Hydrogen Bonds. *Angew. Chem. Int. Ed.* **2012,** *51,* 6236-6240.

(7) Remsing, R. C.; Wildin, J. L.; Rapp, A. L.; Moyna, G. Hydrogen Bonds in Ionic Liquids Revisited: $^{35/37}$Cl NMR Studies of Deuterium Isotope Effects in 1-*N*-Butyl-3-Methylimidazolium Chloride. *J. Phys. Chem. B* **2007,** *111,* 11619-11621.

(8) Miran, M. S.; Kinoshita, H.; Yasuda, T.; Susan, M. A. B. H.; Watanabe, M. Hydrogen Bonds in Protic Ionic Liquids and their Correlation with Physicochemical Properties. *Chem. Commun.* **2011,** *47,* 12676-12678.

(9) Atkin, R.; Warr, G. G. The Smallest Amphiphiles: Nanostructure in Protic Room-Temperature Ionic Liquids with Short Alkyl Groups. *J. Phys. Chem. B* **2008,** *112,* 4164-4166.

(10) Zahn, S.; Uhlig, F.; Thar, J.; Spickermann, C.; Kirchner, B. Intermolecular Forces in an Ionic Liquid ([Mmim][Cl]) Versus in a Typical Salt (NaCl). *Angew. Chem. Int. Ed.* **2008,** *47,* 3639-3641.

(11) Ohmine, I.; Tanaka, H. Fluctuation, Relaxations, and Hydration in Liquid Water. Hydrogen-Bond Rearrangement Dynamics. *Chem. Rev.* **1993,** 2545-2566.

(12) Laage, D.; Hynes, J. T. A Molecular Jump Mechanism of Water Reorientation. *Science* **2006,** *311,* 832-835.

(13) Buchner, R.; Hefter, G. Interactions and Dynamics in Electrolyte Solutions by Dielectric Spectroscopy. *Phys. Chem. Chem. Phys.* **2009,** *11,* 8984-8999.

(14) Nibbering, E. T. J.; Elsaesser, T. Ultrafast Vibrational Dynamics of Hydrogen Bonds in the Condensed Phase. *Chem. Rev.* **2004,** *104,* 1887-1914.

(15) Bakker, H. J.; Skinner, J. L. Vibrational Spectroscopy as a Probe of Structure and Dynamics in Liquid Water. *Chem. Rev.* **2010,** *110,* 1498-1517.

(16) Schröder, C.; Sonnleitner, T.; Buchner, R.; Steinhauser, O. The Influence of Polarizability on the Dielectric Spectrum of the Ionic Liquid 1-Ethyl-3-Methyl-Imidazolium Triflate. *Phys. Chem. Chem. Phys.* **2011,** *13,* 12240-12248.

(17) Turton, D. A.; Sonnleitner, T.; Ortner, A.; Walther, M.; Hefter, G.; Buchner, R.; Wynne, K. Structure and Dynamics in Protic Ionic Liquids: A Combined Ultrafast Optical Kerr Effect (OKE) & Dielectric Study. *Faraday Discuss.* **2012,** *154,* 145-153.

(18) Weingärtner, H.; Knocks, A.; Schrader, E.; Kaatze, U. Dielectric Spectroscopy of the Room Temperature Molten Salt Ethylammonium Nitrate. *J. Phys. Chem. A* **2001,** *105,* 8646-8650.

(19) Krüger, M.; Bründermann, E.; Funkner, S.; Weingärtner, H.; Havenith, M. Polarity Fluctuations of the Protic Ionic Liquid Ethylammonium Nitrate in the Terahertz Regime. *J. Chem. Phys.* **2010,** *132,* 101101.

(20) Zeroka, D.; Jensen, J. O.; Samuels, A. C. Infrared Spectra of Some Isotopomers of Ethylamine and the Ethylammonium Ion: A Theoretical Study. *J. Mol. Struct.: THEOCHEM* **1999,** *465,* 119-139.

(21) Schäfer, T.; Kandratsenka, A.; Vöhringer, P.; Schroeder, J.; Schwarzer, D. Vibrational Energy Relaxation of the ND-Stretching Vibration of NH_2D in Liquid NH_3. *Phys. Chem. Chem. Phys.* **2012,** *14,* 11651-11656.

(22) Liu, L.; Hunger, J.; Bakker, H. J. Energy Relaxation Dynamics of the Hydration Complex of Hydroxide. *J. Phys. Chem. A* **2011,** *115,* 14593-14598.

(23) We have calculated the macroscopic heat diffusivity of EAN from its thermal conductivity[34] and the heat capacity.[35]

(24) Yoshida, K.; Iwata, K.; Nishiyama, Y.; Kimura, Y.; Hamaguchi, H. Local Structures in Ionic Liquids Probed and Characterized by Microscopic Thermal Diffusion Monitored with Picosecond Time-Resolved Raman Spectroscopy. *J. Chem. Phys.* **2012,** *136,* 104504.

(25) Note that the underestimation of the thermal diffusivity (compared to the macroscopic value) in our model cannot lead to low $\tau_{\mathrm{DR}}/\tau_{\mathrm{IR}}$ ratios. Higher values for χ would yield even longer τ_{IR} values, thus making $\tau_{\mathrm{DR}}/\tau_{\mathrm{IR}}$ even smaller.

(26) Böttcher, C. F. J. *Theory of Electric Polarization;* Volume 1 and 2 Elsevier: Amsterdam, 1978.

(27) Hardy, E. H.; Zygar, A.; Zeidler, M. D.; Holz, M.; Sacher, F. D. Isotope Effect on the Translational and Rotational Motion in Liquid Water and Ammonia. *J. Chem. Phys.* **2001,** *114,* 3174-3181.

(28) Fish, K.; Miller, R. C.; Smyth, C. P. Microwave Absorption and Molecular Structure in Liquids. XXIV. The Dielectric Relaxation of Liquid Ammonia. *J. Chem. Phys.* **1958,** *29,* 745-746.

(29) Hunger, J.; Stoppa, A.; Schrödle, S.; Hefter, G.; Buchner, R. Temperature Dependence of the Dielectric Properties and Dynamics of Ionic Liquids. *ChemPhysChem* **2009,** *10,* 723-733.

(30) Shim, Y.; Kim, J. K. Dielectric Relaxation, Ion Conductivity, Solvent Rotation, and Solvation Dynamics in a Room-Temperature Ionic Liquid. *J. Phys. Chem. B* **2008,** *112,* 11028-11038.

(31) Turton, D. A.; Hunger, J.; Stoppa, A.; Hefter, G.; Thoman, A.; Walther, M.; Buchner, R.; Wynne, K. Dynamics of Imidazolium Ionic Liquids from a Combined Dielectric Relaxation and Optical Kerr Effect Study: Evidence for Mesoscopic Aggregation. *J. Am. Chem. Soc.* **2009,** *131,* 11140-11146.

(32) Note that the exact value of α may differ slightly, since DS measures the collective rotation time. The corresponding microscopic rotation time taking local field effects into account is slightly shorter giving even larger jump angles α.

(33) Zahn, S.; Thar, J.; Kirchner, B. Structure and Dynamics of the Protic Ionic Liquid Monomethylammonium Nitrate ($[CH_3NH_3][NO_3]$) from Ab Initio Molecular Dynamics Simulations. *J. Chem. Phys.* **2010,** *132,* 124506.

(34) Bonetti, M.; Nakamae, S.; Roger, M. A Simply Designed Cell for Thermal Conductivity Measurements of Low Vapor Pressure Liquids. *Rev. Sci. Instrum.* **2011,** *82,* 64906.

(35) Allen, M.; Evans, D. F.; Lumry, R. Thermodynamic Properties of the Ethylammonium Nitrate + Water System: Partial Molar Volumes, Heat Capacities, and Expansivities. *J. Solution Chem.* **1985,** *14,* 549-560.

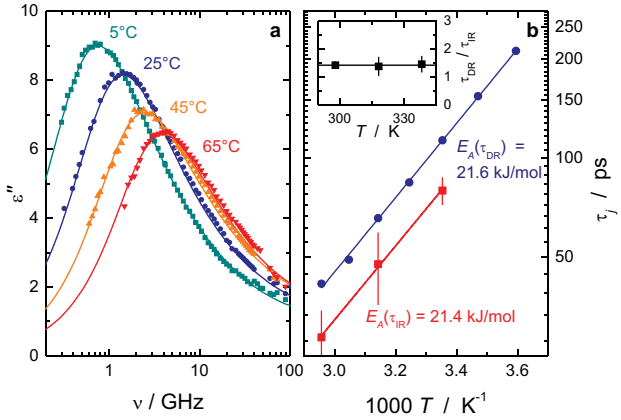

Figure 1: (a) Dielectric loss spectra, $\varepsilon''(\nu)$, for neat EAN (other temperatures omitted for visual clarity). The symbols represent the experimental data, the lines represent fits obtained with a dielectric relaxation model (see SI). (b) Rotational correlation times obtained from fs-IR experiments (τ_{IR}, red squares) and DR spectroscopy (τ_{DR}, blue circles). The lines result from a fit of the data to an Arrhenius model. The inset shows the ratio $\tau_{\mathrm{DR}}/\tau_{\mathrm{IR}}$ measured at three different temperatures. The line in the inset indicates a constant ratio of 1.4.

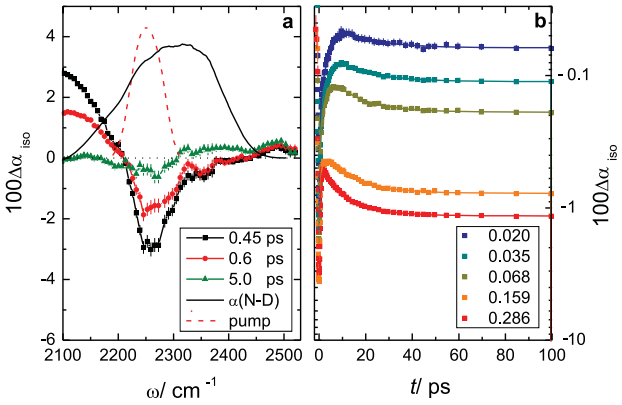

Figure 2: (a) Isotropic transient absorption spectra, $\Delta\alpha_{\mathrm{iso}}(\omega)$ at short delay times, t, (symbols) for $x = 0.035$ at 25 °C. The solid black line shows the ND absorption band corrected for the background absorption of EAN, the dashed red line corresponds to the pump pulse spectrum. (b) Isotropic transient signal, $\Delta\alpha_{\mathrm{iso}}(t)$, at $\omega = 2250\,\mathrm{cm}^{-1}$ for different isotopic exchange ratios, x, at 25 °C. The symbols represent the experimental data and the solid lines show fits obtained with a vibrational relaxation model (see SI, Fig. S3).

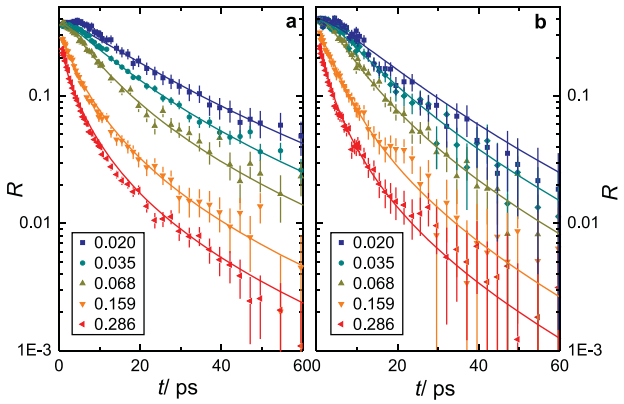

Figure 3: Anisotropy parameter, $R(t)$, at ND stretching frequencies ($\omega = 2250\,\mathrm{cm}^{-1}$), for different isotopic exchange ratios, x, at (a) 25 °C and (b) 45 °C. The symbols represent the experimental data, the lines correspond to fits to the heat-diffusion and molecular reorientation model described in the text.

Hydration Dynamics of Hyaluronan and Dextran

Johannes Hunger,*,‡ Anja Bernecker,† Huib J. Bakker,* Mischa Bonn,*,‡ Ralf P. Richter†,§

*FOM Institute AMOLF, Science Park 104, 1098 XG Amsterdam, The Netherlands
‡Max Planck Institute for Polymer Research, Ackermannweg 10, 55128 Mainz, Germany
†CIC biomaGUNE, Paseo Miramon 182, 20009 Donostia - San Sebastian, Spain
§Max Planck Institute for Intelligent Systems, Heisenbergstrasse 3, 70569 Stuttgart, Germany

Supporting Material

Materials

Hyaluronic acid sodium salt (hyaluronan) from rooster comb (molecular weight 1 to $4 \cdot 10^6\,\mathrm{g\,mol^{-1}}$) and dextran from *Leuconostoc mesenteroides* (analytic standard grade, molecular weight $1.4 \cdot 10^6\,\mathrm{g\,mol^{-1}}$, $\sim 5\,\%$ branched) were purchased from Sigma Aldrich and used without further purification. Samples with different weight fractions, w, (g of polysaccharide / g of solution) were prepared using an analytical balance. Dextran was dissolved in ultrapure water at the desired concentrations and shaken for 2 h at room temperature. Hyaluronan was dissolved in ultrapure water and shaken overnight at 40 °C. The hyaluronic acid salt samples were centrifuged several times for 10 min at 10000 rpm to obtain a homogeneous solution. For fs-IR experiments a small amount ($\sim 4\,\%$ (w/w)) deuterium oxide (99.97 %D from Euriso-top, Saint-Aubin, France) was added to the ultrapure water before dissolving dextran or hyaluronan. Due to fast isotopic exchange, we obtain the equilibrium distribution of deuterium atoms among all acidic protons. Therefore the dominant isotopically labeled species are HOD molecules.

For analysis of the Terahertz experiments, molar concentrations (in $\mathrm{mol\,L^{-1}}$) of water, $c_{\mathrm{H_2O}}$, in the sample are required. These were calculated from the weight fractions, w, using solution densities, ρ, interpolated from literature ($\rho(\mathrm{dextran}) = (997.05 + 410 \cdot w)\,\mathrm{g\,L^{-1}}$; $\rho(\mathrm{HA}) = (997.05 + 440 \cdot w)\,\mathrm{g\,L^{-1}}$) [1, 2, 3].

Polarization-resolved femtosecond-infrared spectroscopy

Experimental method

Femtosecond infrared pump and probe pulses were generated via a sequence of nonlinear optical conversion processes that are pumped by a commercial Ti:sapphire regenerative amplified laser system (Spectra-Physics Hurricane, USA). This system delivers pulses at 800 nm with a duration of 100 fs at a repetition rate of 1 kHz (1 mJ per pulse). Approximately 0.7 mJ of pulse energy is used to pump an optical parametric amplifier (OPA) based on a β-barium borate (BBO) crystal. The OPA is used to generate idler pulses at $\sim 2\,\mu$m, which are subsequently frequency-doubled in a second BBO crystal, yielding pulses at $\sim 1\,\mu$m. In a second parametric amplification process in a lithium niobate crystal the 1 μm pulses are used as a seed and the remaining 800 nm pulses (0.3 mJ) as a pump to generate mid-infrared pulses with a duration of ~ 150 fs and an energy of $\sim 6\,\mu$J. The frequency of these pulses is centered at $2500\,\mathrm{cm^{-1}}$, which coincides with the absorption of the O-D stretching vibration of HOD molecules (Note that the N-D stretch vibration, which is formed via isotopic exchange with HOD absorbs at similar wavenumbers. Its contribution to our experiments, however, is negligible [4]).

A CaF_2 wedged window is used to split the mid-infrared pulses into a pump ($\sim 92\,\%$), a probe ($\sim 4\,\%$), and a reference ($\sim 4\,\%$) pulse. The polarization of the pump pulse is rotated by 45 ° with respect to the probe and the reference polarization using a $\lambda/2$ plate. The time delay of the probe pulses with respect to the pump is varied via a variable path-length delay line. The pump pulse is modulated using

an optical chopper. The three pulses are focused into the sample with an off-axis parabolic mirror. In the sample, which is held between two CaF_2 windows, the foci of the probe and pump-pulse overlap. After passing a polarizer that allows us to select the parallel or perpendicular (with respect to the pump) polarization components, the probe and reference beams are sent into a spectrometer dispersing the beams on a liquid-nitrogen-cooled mercury-cadmium telluride detector. The probe pulse is used to measure the (pump-induced) transient absorption in the sample parallel ($\Delta\alpha_{\parallel}(\omega, t)$) and perpendicular ($\Delta\alpha_{\perp}(\omega, t)$) to the pump polarization as a function of delay time, t, and wavenumber, ω. The reference pulse is used for a spectrally resolved correction of the pulse to pulse energy fluctuations [5].

Data Analysis

From the measured absorption changes $\Delta\alpha_{\parallel}(\omega, t)$ and $\Delta\alpha_{\perp}(\omega, t)$ we construct the isotropic signal:

$$\Delta\alpha_{\mathrm{iso}}(\omega, t) = \frac{\Delta\alpha_{\parallel}(\omega, t) + 2\Delta\alpha_{\perp}(\omega, t)}{3} \tag{S1}$$

The isotropic signal is independent of reorientation processes and is dominated by the vibrational relaxation of the excitation and by the dynamics of any consecutive processes. At short delays the isotropic signal is dominated by the vibrational excitation of the OD oscillators. The vibrational energy relaxes to an intermediate state (i.e. intermediate energy levels) and eventually leads to heating of the sample by a few degrees (low energy levels) [6, 7, 8]. At long delay times ($t > 20\,\mathrm{ps}$) this heating effect prevails. To obtain the anisotropy dynamics, $R(t)$ of the excited OD-stretch transition dipoles, we correct the measured signals $\Delta\alpha_{\parallel}(\omega, t)$ and $\Delta\alpha_{\perp}(\omega, t)$ for this time-dependent thermalization of the sample. The evolution of the thermalization is obtained via detailed analysis of $\Delta\alpha_{\mathrm{iso}}(\omega, t)$ following the route described in detail in Ref. [9]. To briefly summarize, we fit a kinetic model to the isotropic data. In this model the pump pulse generates a population in the first vibrational excited state. This excitation transiently populates an intermediate state with a characteristic time constant of $\sim 1.7\,\mathrm{ps}$. For the present samples this time is virtually constant at all concentrations of polysaccharide. The intermediate state has the same absorption spectrum as the vibrational ground state (i.e. the transient absorption equals zero). The intermediate state further relaxes to the final thermal state with a characteristic time constant of $\sim 1\,\mathrm{ps}$ for solutions of 8 % HOD in H_2O. For the present samples this equilibration time is increasing smoothly as the concentration of polysaccharide increases. At the highest concentration (20 % (w/w)) of polysaccharide the equilibration occurs on a $\sim 1.5\,\mathrm{ps}$ timescale. This slow-down of the equilibration indicates a slower equilibration of the samples to the thermal disturbance and/or the appearance of additional intermediate energy levels.

From this analysis, the spectral signature and the temporal evolution of the thermalization is obtained, which is subsequently subtracted from the raw transient spectra ($\Delta\alpha_{\parallel}(\omega, t)$ and $\Delta\alpha_{\perp}(\omega, t)$). The thus obtained corrected transient spectra, $\Delta\alpha'_{\parallel}(\omega, t)$ and $\Delta\alpha'_{\perp}(\omega, t)$ solely reflect the signal originating from of the excited OD oscillators.

From the corrected signals we construct the anisotropy parameter $R(t)$:

$$R(\omega, t) = \frac{\Delta\alpha'_{\parallel}(\omega, t) - \Delta\alpha'_{\perp}(\omega, t)}{\Delta\alpha'_{\parallel}(\omega, t) + 2\Delta\alpha'_{\perp}(\omega, t)}. \tag{S2}$$

$R(t)$ directly corresponds to the second order rotational correlation time of the excited OD oscillators. $R(t)$ decays are averaged over frequencies ranging from $2460\,\mathrm{cm}^{-1}$ to $2540\,\mathrm{cm}^{-1}$ as it is independent of absorption frequency [9].

The thus obtained anisotropies are inconsistent with all water molecules having the same rotational dynamics (as for neat water [7]), which is described by a single exponential decay of $R(t)$ (see Figure S1). Hence, we model the experimental anisotropies with a double exponential decay (eq 1), which excellently describes the observed rotational dynamics of the HOD molecules (see Figures 1 & S1). From these fits we obtain a rotational correlation time of $\tau_{\mathrm{s,IR}} \gg 10\,\mathrm{ps}$ at all concentrations, if all parameters of eq 1 are allowed to vary. This means that the rotational dynamics of the slow subensemble of water molecules are essentially static on the 5 ps time-scale of our experiment. To reduce the number of free parameters, we fix the rotation times of the slowed down subsensmble of water to $\tau_{\mathrm{s,IR}} \approx \infty$ ($t/\tau_{\mathrm{s,IR}} \approx 0$).

Terahertz time-domain spectroscopy

Experimental method

Terahertz pulses are generated in a ZnTe (110) nonlinear crystal [10] from 800 nm pulses with a duration of $\sim$ 150 fs from a Ti:Sapphire laser (Coherent Legend Elite, USA). The generated THz pulses have a duration of $\sim$ 1 ps. The time-dependent electric field of the THz pulse is measured via its electro-optic effect on a variably delayed 800 nm laser pulse in a second ZnTe crystal. A frequency domain analysis of the THz pulse transmitted through an empty cell and the THz pulse transmitted through a filled sample cell, yields the frequency dependent complex index of refraction ($\hat{n}(\nu) = n(\nu) - \mathrm{i}k(\nu)$) as function of field frequency, ν (ranging from 0.4 to 1.2 THz). In analysing the data, all (multiple) reflection and transmission coefficients for all transitions (air-window-sample-window-air) were taken into account [11]. To minimize the effect of fluctuations in the THz intensity, a rotating sample cell with two separate sample compartments is used to position the sample and a pure water reference alternatingly in the focus of the THz beam. The sample is held between two Polychlorotrifluoroethylene (PCTFE) windows separated by a teflon spacer (thickness $\sim 100\,\mu$m). The neat water data were used to calibrate the spectra of the samples.

Data Analysis

Complex refractive index spectra were converted to complex permittivity spectra, $\hat{\varepsilon}(\nu)$ ($= \hat{n}^2(\nu)$). For neat water $\hat{\varepsilon}(\nu)$ is dominated by an intense relaxation mode at $\sim$ 20 GHz that can be well described with a Debye equation (i.e. a single exponential decay of the orientational polarization of the sample in the time-domain) [12]. This relaxation originates from the partial alignment of the (dipolar) water molecules to the external electric field. For neat water a characteristic collective first-order orientational relaxation time of $\tau_1 = 8.3$ ps is observed at ambient temperature [12]. Its amplitude is found to be $S_1 = 72$. Further, a weak Debye-type high-frequency mode centered at ~ 0.5 THz is observed with an amplitude $S_2 \approx 1.3$ and relaxation time $\tau_2 \approx 200$ fs. Thus, we model the experimental spectra with a superposition of two Debye-type relaxation modes:

$$\hat{\varepsilon}(\nu) = \frac{S_1}{1 + 2\pi\nu\mathrm{i}\tau_1} + \frac{S_2}{1 + 2\pi\nu\mathrm{i}\tau_2} + \varepsilon_\infty \tag{S3}$$

where ε_∞ represents the high-frequency limit of the permittivity. It subsumes all electronic and intramolecular polarizations at infrared and optical frequencies. Following previous work [13], τ_1 was fixed to the value obtained from the reference sample (pure water) using the known static permittivity of water, $\varepsilon = S_1 + S_2 + \varepsilon_\infty = 78.368$ [14]. τ_2, S_1, S_2, and ε_∞ are the independent fit parameters. The thus obtained amplitude S_1 can be converted to the molar concentration of unaffected (bulk-like) water molecules, c_b using the Cavell equation [15, 16]:

$$c_\mathrm{b} = \frac{k_\mathrm{B} T \varepsilon_0}{N_\mathrm{A}} \frac{2\varepsilon + 1}{\varepsilon} \cdot S_1 \cdot \frac{1}{\mu_\mathrm{eff}^2} \tag{S4}$$

where N_A and k_B are the Avogadro and Boltzmann constant, respectively and T is the thermodynamic temperature. μ_eff is the effective dipole moment of water in solution. μ_eff was assumed to be constant and the same as for neat water $\mu_\mathrm{eff} = 3.8$ D (1 D $= 3.33564 \times 10^{-30}$ Cm) [12, 17].

Supporting Figure

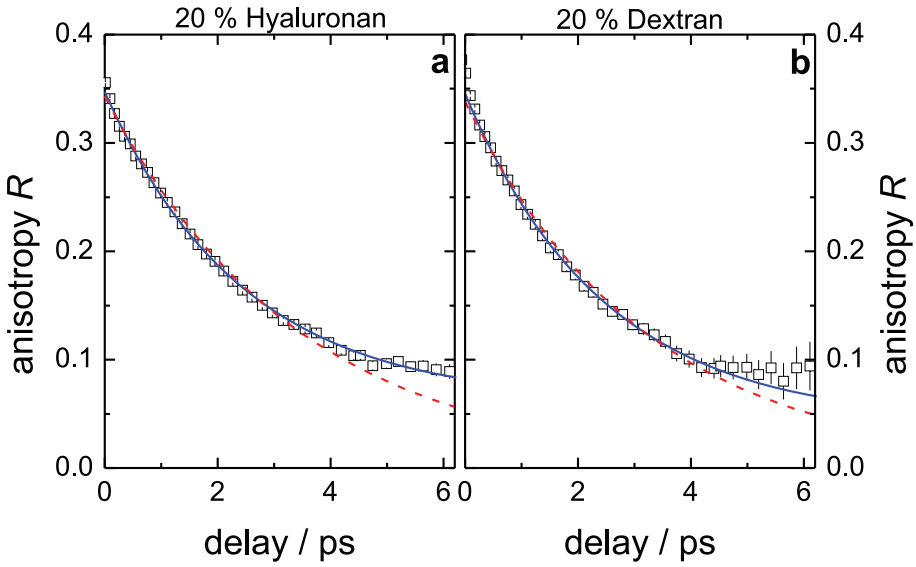

Figure S1: Anisotropy parameter, $R(t)$, for the OD stretch vibration for solutions of 20 % hyaluronan (a) and 20 % dextran (b) in isotopically diluted water (8 % HOD in H_2O). Dashed red lines correspond to fits of a single exponential decay to the experimental data. Solid blue lines show the fits with a double exponential decay (eq 1).

References

[1] Gómez-Alejandre, S., E. Sánchez de la Blanca, C. Abradelo de Usera, M. F. Rey-Stolle, and I. Hernández-Fuentes. 2000. Partial specific volume of hyaluronic acid in different media and conditions. *Int. J. Biol. Macromol.* 27:287–290.

[2] Kany, H.-P., H. Hasse, and G. Maurer. 1999. Thermodynamic properties of aqueous dextran solutions from laser-light-scattering, membrane osmometry, and isopiestic measurements. *J. Chem. Eng. Data*. 44:230–242.

[3] Akashi, N., J.-I. Kushibiki, and F. Dunn. 2000. Measurements of acoustic properties of aqueous dextran solutions in the VHF/UHF range. *Ultrasonics*. 38:915–919.

[4] Rezus, Y. L. A., and H. J. Bakker. 2006. Effect of urea on the structural dynamics of water. *Proc. Natl. Acad. Sci. U.S.A.* 103:18417–18420.

[5] Bakker, H. J., Y. L. A. Rezus, and R. L. A. Timmer. 2008. Molecular reorientation of liquid water studied with femtosecond mid-infrared spectroscopy. *J. Phys. Chem. A*. 112:11523–11534.

[6] Steinel, T., J. B. Asbury, J. Zheng, and M. D. Fayer. 2004. Watching hydrogen bonds break: A transient absorption study of water. *J. Phys. Chem. A*. 108:10957–10964.

[7] Rezus, Y. L. A., and H. J. Bakker. 2006. Orientational dynamics of isotopically diluted H_2O and D_2O. *J. Chem. Phys.* 125:144512.

[8] Bakker, H. J., and J. L. Skinner. 2010. Vibrational spectroscopy as a probe of structure and dynamics in liquid water. *Chem. Rev.* 110:1498–1517.

[9] Rezus, Y. L., and H. J. Bakker. 2005. On the orientational relaxation of HDO in liquid water. *J. Chem. Phys.* 123:114502.

[10] Ahn, J., A. V. Efimov, R. D. Averitt, and A. J. Taylor. 2003. Terahertz waveform synthesis via optical rectification of shaped ultrafast laser pulses. *Opt. Express*. 11:2486–2496.

[11] Knoesel, E., M. Bonn, J. Shan, F. Wang, and T. F. Heinz. 2004. Conductivity of solvated electrons in hexane investigated with terahertz time-domain spectroscopy. *J. Chem. Phys.* 121:394-404.

[12] Fukasawa, T., T. Sato, J. Watanabe, Y. Hama, W. Kunz, and R. Buchner. 2005. Relation between dielectric and low-frequency Raman spectra of hydrogen-bond liquids. *Phys. Rev. Lett.* 95:197802.

[13] Tielrooij, K. J., R. L. A. Timmer, H. J. Bakker, and M. Bonn. 2009. Structure dynamics of the proton in liquid water probed with terahertz time-domain spectroscopy. *Phys. Rev. Lett.* 102:198303.

[14] Fernández, D. P., A. R. H. Goodwin, E. W. Lemmon, J. M. H. Levelt Sengers, and R. C. Williams. 1997. A formulation of the static permittivity of water and steam at temperatures from 283 K to 873 K at pressures up to 1200 MPa, including derivatives and Debye–Hückel coefficients. *J. Phys. Chem. Ref. Data*. 26:1125–1166.

[15] Cavell, E. A. S., P. C. Knight, and M. A. Sheikh. 1971. Dielectric relaxation in non aqueous solutions. part 2. Solutions of tri(n-butyl)ammonium picrate and iodide in polar solvents. *Trans. Faraday Soc.* 67:2225–2233.

[16] Hunger, J., A. Stoppa, R. Buchner, and G. Hefter. 2009. Dipole correlations in the ionic liquid 1-N-ethyl-3-N-methylimidazolium ethylsulfate and its binary mixtures with dichloromethane. *J. Phys. Chem. B*. 113:9527– 9537.

[17] Hunger, J., K. J. Tielrooij, R. Buchner, M. Bonn, and H. J. Bakker. 2012. Complex formation in aqueous trimethylamine-N-oxide (TMAO) solutions. *J. Phys. Chem. B*. 116:4783–4795.